International Journal of Pharmaceutics 613 (2022) 121361

Contents lists available at ScienceDirect

International Journal of Pharmaceutics

journal homepage: www.elsevier.com/locate/ijpharm

Ocular metabolism and distribution of drugs in the rabbit eye: Quantitative assessment after intracameral and intravitreal administrations

Eva M. del Amo [a,*], Anam Hammid [a], Melanie Tausch [b], Elisa Toropainen [a], Amir Sadeghi [a], Annika Valtari [a], Jooseppi Puranen [a], Mika Reinisalo [a], Marika Ruponen [a], Arto Urtti [a,c,d], Achim Sauer [e], Paavo Honkakoski [a]

[a] University of Eastern Finland, School of Pharmacy, Biopharmaceutics, Yliopistonranta 1, 70210 Kuopio, Finland
[b] NUVISAN GmbH, Am Feld 32, 85567 Grafing, Germany
[c] University of Helsinki, Faculty of Pharmacy, Drug Research Program, Yliopistonkatu 3, 00014 Helsinki, Finland
[d] Saint-Petersburg State University, Institute of Chemistry, Universitetskiy Prospekt, 26, Petergoff 198504, Russian Federation
[e] Department of Drug Discovery Sciences, Boehringer Ingelheim Pharma GmbH & Co. KG, 88397 Biberach, Germany

ARTICLE INFO

Keywords:
Ocular tissues
Acetaminophen
Brimonidine
Cefuroxime
Sunitinib
Sulfotransferase
Aldehyde oxidase
Esterase
CYP3A
Rabbit
Metabolism
Ocular pharmacokinetics

Chemical compounds studied in the article:
Acetaminophen
Acetaminophen sulfate
Brimonidine tartrate
Brimonidine-2,3-dione
Cefuroxime axetil
Cefuroxime
Sunitinib malate
N-Desethyl sunitinib
Ketoconazol
2-Oxobrimonidine

ABSTRACT

Quantitation of ocular drug metabolism is important, but only sparse data is currently available. Herein, the pharmacokinetics of four drugs, substrates of metabolizing enzymes, was investigated in albino rabbit eyes after intracameral and intravitreal administrations. Acetaminophen, brimonidine, cefuroxime axetil, and sunitinib and their corresponding metabolites were quantitated in the cornea, iris-ciliary body, aqueous humor, lens, vitreous humor, and neural retina with LC-MS/MS analytics. Non-compartmental analysis was employed to estimate the pharmacokinetic parameters of the parent drugs and metabolites. The area under the curve (AUC) values of metabolites were 12–70 times lower than the AUC values of the parent drugs in the tissues with the highest enzymatic activity. The ester prodrug cefuroxime axetil was an exception because it was efficiently and quantitatively converted to cefuroxime in the ocular tissues. In contrast to the liver, sulfotransferases, aldehyde oxidase, and cytochrome P450 3A activities were low in the eye and they had negligible impact on ocular drug clearance. With the exception of esterase substrates, metabolism seems to be a minor player in ocular pharmacokinetics. However, metabolites might contribute to ocular toxicity, and drug metabolism in various eye tissues should be investigated and understood thoroughly.

Abbreviations: AH, aqueous humor; AOX, aldehyde oxidase; $AUC_{0-\infty}$, area under the curve from time zero to infinity; $AUC_{0-tlast}$, the area under the curve from time zero until the last sampling point; $AUC_{t1-tlast}$, the area under the curve from first sampling point until the last sampling point; CES, carboxylesterase; CL_{ic}, intracameral clearance; CL_{ivt}, intravitreal clearance; CYP, cytochrome P450; DMEs, drug-metabolizing enzymes; IC, intracameral; ICB, iris-ciliary body; ISTD, internal standards; IVT, intravitreal; K_p, partition coefficient; LLOQ, lower limit of quantification; Log $D_{7.4}$, logarithm of the octanol-water distribution coefficient at pH 7.4; NCA, non-compartmental analysis; SE, standard error of estimates; SULT, sulfotransferase; $t_{1/2}$, elimination half-life; UGT, UDP-glucuronyltransferase; VH, vitreous humor; V_{ic}, intracameral volume of distribution; V_{ivt}, intravitreal volume of distribution; ULOQ, upper limit of quantification.

* Corresponding author.
E-mail address: eva.delamo@uef.fi (E.M. del Amo).

https://doi.org/10.1016/j.ijpharm.2021.121361
Received 11 October 2021; Received in revised form 2 December 2021; Accepted 4 December 2021
Available online 9 December 2021

1. Introduction

Metabolism of a drug is usually assessed by standard assays that inform on its metabolic stability, identity of its metabolites, and enzymatic routes of metabolism. These assays employ liver microsomes, S9 fractions, or hepatocytes from humans and animals as enzyme sources although species differences (Dalgaard, 2015; Martignoni et al., 2006) may complicate the translation of results from animal studies to the human situation. The repertoire of drug-metabolizing enzymes (DMEs) in extrahepatic tissues, such as the eye, are narrower and their expression much lower than those in the liver (Argikar et al., 2017; Jhajra et al., 2012), if at all accurately established. Therefore, the rate of formation and relative proportions of ocular metabolites may differ significantly from the systemic metabolite profile.

Numerous DMEs have been reported in human and animal ocular tissues (reviewed by Ahmad et al., 2018; Argikar et al., 2017; Attar et al., 2005; Dumouchel et al., 2018). Oxidative, reductive and hydrolytic (phase I) and conjugative (phase II) enzymes are present at mRNA, protein, and activity levels in ocular tissues (Ahmad et al., 2018; Argikar et al., 2017; Dumouchel et al., 2018; Duvvuri et al., 2004; Kölln and Reichl, 2012; Nakano et al., 2014; Watkins et al., 1991; Zhang et al., 2008). However, detailed information of isoenzyme distribution, absolute expression levels, and quantitative impact on ocular pharmacokinetics are scant or non-existent.

Many pre-clinical and clinical ocular therapeutics are potential substrates for these enzymes. For example, bioactivation of prodrugs cefuroxime axetil, loteprednol etabonate, acyclovir, dipivefrin, and latanoprost (Druzgala et al., 1991; Duvvuri et al., 2004; Harding et al., 1984; Redell et al., 1983; Sjöquist et al., 1998) is catalyzed by esterases. Aldehyde oxidase (AOX) is involved in the biotransformation of methotrexate, brimonidine, and ripasudil (Acheampong et al., 1995, 2002a; Joussen et al., 1999; Testa et al., 2020). Ketoconazole, sunitinib, and cyclosporine A (Cirello et al., 2017; Speed et al., 2012; Van Herwaarden et al., 2005) are oxidized by cytochrome P450s (CYPs) while moxifloxacin (Muijsers and Jarvis, 2002), ketorolac (Vadivelu et al., 2015), and acetaminophen (Romanelli et al., 1991) are substrates for conjugating enzymes.

The invasive sampling of ocular tissues often precludes direct evaluation of human ocular metabolism. Enzymatic studies of human eyes are not common (Ahmad et al., 2018) and most results are derived from cell cultures (Kölln and Reichl, 2012) with unclear relevance to the *in vivo* situation (Cirello et al., 2017) or post-mortem tissues with the issue of enzyme degradation (Zhang et al., 2008). Consequently, ocular pharmacokinetic studies rely on laboratory animals, particularly rabbits. A good correlation is observed between human and rabbit pharmacokinetic parameters after intravitreal injection. Hence, the rabbit has been proposed as a promising translational model to human eye due to close similarity in some anatomical and physiological parameters, and scalable in some others (del Amo et al., 2017; Del Amo and Urtti, 2015).

In the present article, we aim to investigate quantitatively ocular pharmacokinetics of four selected drugs (Appendix A Table S1) reported to be substrates of ocular enzymes in different species: acetaminophen, brimonidine, cefuroxime axetil, and sunitinib. Acetaminophen and cefuroxime axetil are commonly administered orally for analgesic and antibiotic purposes, respectively. Cefuroxime axetil is a prodrug, and the active form is cefuroxime (called "metabolite" here for the sake of simplicity). On the other hand, brimonidine is an α_2 adrenergic receptor agonist used in ophthalmic topical administration for the management of glaucoma. It also exerts neuroprotective effects and is currently in clinical trials formulated as an intravitreal implant for the treatment of geographic age-related macular degeneration (AMD) (NCT00658619, NCT02087085). Sunitinib is an inhibitor of receptor tyrosine kinases (such as the vascular endothelial growth factor receptor) and has been used as an oral anticancer agent. Presently, an intravitreal depot injectable for sunitinib is in a clinical trial for the treatment of wet AMD (NCT03953079).

The four compounds were dosed in a single injection solution and injected intracamerally (IC) or intravitreally (IVT) into the rabbit eye (Fig. 1). Care was taken to avoid that these substrates could be metabolized by more than one enzyme. Sunitinib is oxidized primarily by CYP3A, cefuroxime axetil hydrolyzed by esterases, acetaminophen predominantly conjugated by UDP-glucuronyltransferases (UGT) and sulfotransferases (SULT), and brimonidine oxidized mainly by AOX but to a lesser extent by unknown hepatic CYPs. However, brimonidine is not reported to inhibit DMEs. Therefore, we do not expect any metabolic interactions between the four co-administrated drugs.

The concentration–time profiles of the drugs and the corresponding metabolites in six different ocular tissues (Fig. 1) were evaluated by non-compartmental pharmacokinetic analysis to assess the impact of metabolism on the drug ocular clearance, and the distribution on the ocular pharmacokinetics.

2. Materials and methods

2.1. In vivo experiments

2.1.1. Preparation of drug cocktail

The drug cocktail containing 3 mM acetaminophen (Sigma), 3 mM brimonidine tartrate (MedChemExpress, Sweden), 1 mM cefuroxime axetil (Toronto Research Chemicals, Canada), and 3 mM sunitinib malate (USP reference standard, Sigma Aldrich) was prepared in Dulbecco's phosphate-buffered saline (DPBS, ThermoFisher Scientific). The pH of the solution was adjusted with 1 N NaOH solution to 6.5 and stored at + 4 °C overnight until used in rabbit studies.

2.1.2. Animals

Twelve three-month-old male New Zealand White rabbits (Charles River Laboratories, UK) weighing 3.0–3.4 kg were used in the experiment. The animals were housed in individual cages in a temperature- and humidity-controlled environment with 12 h dark-light cycles and fed with a normal pellet diet with water *ad libitum*. Before being accepted to the study, animals underwent a thorough examination to confirm ocular health. Animal experiments were carried out at the University of Eastern Finland and were approved by the national Project Authorization Board (ESAVI/27769/2020) and according to the EU directive 2010/63/EU.

The animals were anaesthetized with medetomidine (Domitor vet 1 mg/mL; Orion Pharma, Espoo, Finland; dose 0.5 ml/kg, sc) and ketamine (Ketaminol vet 50 mg/mL; Pfizer Oy Animal Health, Espoo, Finland; dose 0.5 ml/kg, sc), pupils were dilated with tropicamide (Oftan Tropicamid 5 mg/mL; Santen Pharmaceutical Co., Ltd., Tampere, Finland) and the surface of the eye was locally anaesthetized with oxybuprocaine (Oftan Obucain 4 mg/mL; Santen) before injections in both eyes. Half of the rabbits were injected IC (n = 12 eyes) and the other half IVT (n = 12 eyes). After injection, the eyes were moisturized with a carbomer gel (Viscotears 2 mg/g; Dr. Gerhard Mann chem.-pharm. Fabrik GmbH, Berlin, Germany) and the anaesthesia was antagonized with atipamezole (Antisedan vet 5 mg/mL; Orion Pharma, Espoo, Finland; 0.2 ml/kg, sc), when necessary. IC injections (10 μL/eye) were performed with the method by Fayyaz et al. (2020). Here, 31G needles were used for both IC and IVT injections. In IVT injections, the needle was inserted about 4.5 mm out of the corneal limbus in the upper temporal side, through the sclera into the vitreous, and 50 μL of the drug solution was injected into the vitreous at 4 mm depth.

Based on our previous experience with small molecule drugs (Del Amo et al., 2015; Fayyaz et al., 2020), we selected the sampling period to cover at least two half-lives. Such concentration–time profiles allow reasonable estimation of primary pharmacokinetic parameters and compound distribution to neighboring tissues. The animals were sacrificed at designated time points (1, 3, and 5 h after IC injections and 2, 8, and 24 h after IVT injections; n = 4 eyes at every time point) with a lethal dose of pentobarbital (Mebunat vet 60 mg/mL; Orion Pharma,

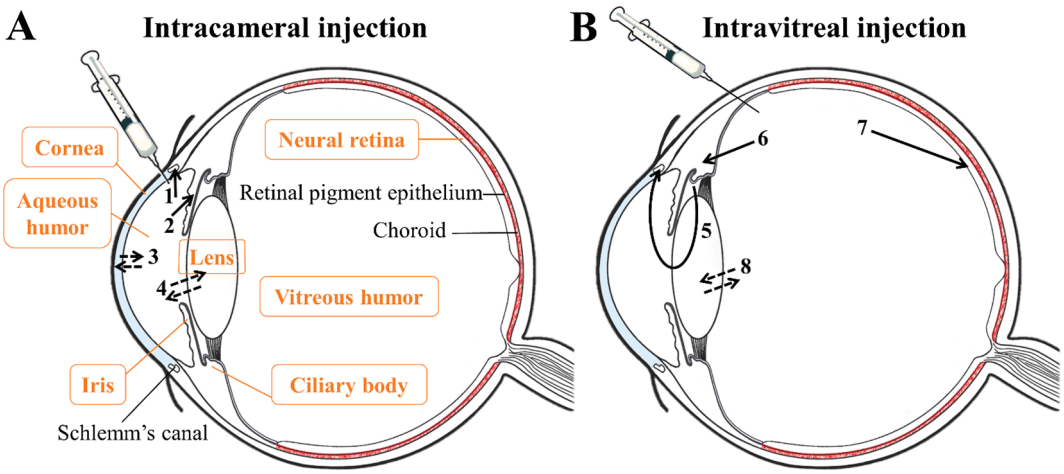

Fig. 1. Schematic representation of the anatomy of the eye and the drug kinetics after IC and IVT administrations, where the investigated tissues for potential enzymatic activity are framed. After IC administration (**A**), the drug is cleared via aqueous humor outflow into Schlemm's canal reaching the venous and lymphatic systems (1), and via permeation into the iris-ciliary body crossing the vascular blood-aqueous barrier into the systemic blood circulation (2). The drug may distribute into the cornea (3) or lens (4). After IVT administration (**B**), the drug is cleared by the aqueous humor outflow to the anterior chamber into Schlemm's canal (5) and posteriorly, reaching the systemic circulation after crossing the blood-aqueous barrier at the iris and ciliary body tissues (6) and the blood-retinal barrier at the retina into the choroidal circulation (7). The drug may distribute into the lens (8).

Espoo, Finland; dose 120 mg/kg) in the marginal ear vein. Both eyeballs were enucleated followed by aqueous humor aspiration and collection of the tissues cornea, iris-ciliary body, lens, the vitreous humor, and neural retina (Fayyaz et al., 2021; Hammid et al., 2021). Aqueous humor and vitreous samples were immediately acidified by adding an equal weight of 0.13 M HCl. The isolated tissues were immediately snap-frozen in liquid nitrogen and stored at −80 °C until analysed.

2.2. LC-MS analysis

2.2.1. Analytes and internal standards for bioanalytical quantification

The analytical reference for acetaminophen, brimonidine tartrate, cefuroxime axetil and sunitinib malate were taken from the same chemical batch used in the *in vivo* experiments. Acetaminophen sulfate and cefuroxime were purchased from Sigma Aldrich (Hamburg, Germany), brimonidine-2,3-dione and N-desethyl sunitinib from Toronto Research Chemicals (Toronto, ON, Canada). The internal standards (ISTD) [$^2H_4$] brimonidine, [$^2H_3$] cefuroxime and [$^2H_{10}$] sunitinib were purchased from Cayman Chemical (Ann Arbor, MI, USA), and [$^2H_4$] acetaminophen was from Sigma Aldrich (Saint Louis, MO, USA).

2.2.2. Sample preparation

To stabilize the analytes, an equal volume (v/w) of 0.13 M HCl was added to the following tissue samples: iris-ciliary body, retina, lens and cornea. Corneal samples were extracted by adding water (1 part, v/w) first, followed by the addition of ethanol (3 parts, v/w) while iris-ciliary body, retina, and lens tissues were extracted by adding four volumes (v/w) of ethanol:water mixture (4 + 1, v/v). These samples were then homogenized with a Precellys® Evolution homogenizer (Bertin Technologies, France). Aqueous and vitreous humor samples were extracted by adding four volumes (v/w) of ethanol:water mixture (4 + 1, v/v), followed by vortexing. All homogenates were centrifuged at 14,200*g* for 5 min at ambient temperature to remove debris.

Cornea homogenates were diluted with the ISTD solution (60 nM of [$^2H_4$] acetaminophen, [$^2H_{10}$]sunitinib, [$^2H_4$]brimonidine and [$^2H_3$] cefuroxime, respectively, in ethanol) and analysed after liquid–liquid extraction with *tert*-butylmethylether (tBME) (50 µL sample + 50 µL ISTD solution + 150 µL tBME), evaporation to dryness using a gentle stream of nitrogen (8 bar) at 40 °C and reconstitution in 10% acetonitrile in water. For all other tissue homogenates, an aliquot was diluted with the ISTD solution, evaporated to dryness, and reconstituted in an adequate amount of 10% acetonitrile in water depending on the calibration range.

2.2.3. LC-MS analysis

The analytes (acetaminophen, sunitinib, brimonidine tartrate, cefuroxime axetil, and their metabolites acetaminophen-sulfate, N-desethyl sunitinib, cefuroxime and brimonidine-2,3-dione, and the corresponding ISTDs) were analysed using a LC-MS system consisting of an Agilent 1290 Infinity II (Agilent Technologies Inc., Santa Clara, California, USA), a CTC PAL3 RSi 534 (CTC Analytics AG, Zwingen, Switzerland) and a Sciex 5500+ triple quadrupole mass spectrometer (AB Sciex, Redwood City, CA, USA).

For ultra-performance liquid chromatography (UPLC) separation, a Luna Omega C18 column (1.6 µm, 2.1 mm × 50 mm, Phenomenex Inc., Torrance, California, USA) was maintained at 40 °C and an eluent flow rate of 0.7 ml/min was used. Eluent A was 0.1% formic acid in water and eluent B was 0.1% formic acid in acetonitrile. The eluent gradient is presented in Table S2 (UPLC gradient).

The injection volume was between 5 and 10 µL. One product ion was monitored for each compound employing multiple reaction monitoring mode (MRM) in positive (experiment 1) and negative mode (experiment 2). The following MS conditions were used: curtain gas (CUR) 35 V, ion spray voltage (IS) 4500 V, collision gas (CAD) 12 V, nebulizer gas (GS1) 50 V, turbo gas (GS2) 70 V, source temperature 500 °C and dwell time 20 ms. MS data were analysed with Analyst®, Version 1.7.1 (AB Sciex, USA). See Table S3 for mass transitions and compound-specific parameters.

Analytical standards and quality control samples were prepared in homogenates of each tissue. The calibration curve with eight concentration levels was prepared in singleton except for the lower limit of quantification (LLOQ) and upper limit of quantification (ULOQ), which were analysed in duplicate at the end of each MS run sequence. Standard curves had 70–130% mean accuracies compared to the nominal concentration. The LLOQ and ULOQ of all analytes and metabolites in all matrices is presented in Table S4.

2.3. Pharmacokinetic analyses

Mean concentration–time profiles of parent drugs and metabolites in the ocular tissues were analysed using non-compartmental analysis (NCA) with Phoenix WinNonlin (build 8.3.1, Certara L.P.) using the

linear up log down calculation method. The pharmacokinetic parameters of clearance and volume of distribution of the parent drugs after IC (CL_{ic} and V_{ic} respectively) and IVT (CL_{ivt} and V_{ivt} respectively) injections were estimated. Moreover, the area under the curve (AUC) from time zero until last sampling point ($AUC_{0\text{-}tlast}$), the AUC from first time sampling point till the last one ($AUCt_1\text{-}t_{last}$), and the total AUC from time zero until infinity ($AUC_{0\text{-}\infty}$), and elimination half-life ($t_{1/2}$) of both parent compound and metabolite were estimated in the six ocular tissues.

The partitioning of the compounds between the dosed tissue (aqueous humor after IC injection and vitreous humor after IVT injection) and the surrounding tissues was determined based on the equation

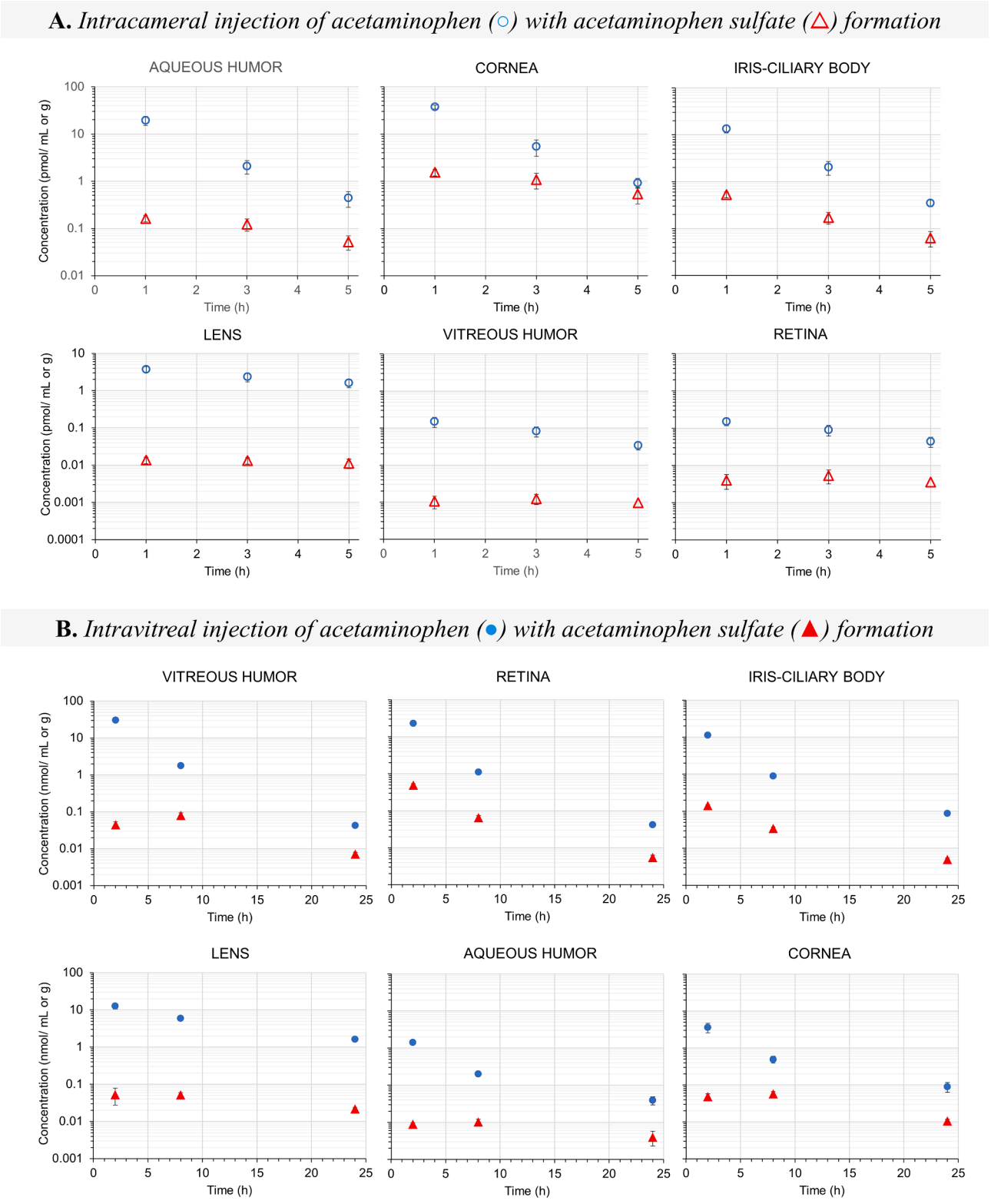

Fig. 2. Concentration-time profiles of acetaminophen (circle) and acetaminophen sulfate (triangle) (mean concentration ± standard error of the mean) after acetaminophen IC (30 nmol, A) and IVT (150 nmol, B) injections.

(1):

$$\text{partition coefficient}\left(K_p\right) = AUC_{0-t\text{last neighbouring tissue}} / AUC_{0-t\text{last dosed tissue}} \quad (1)$$

3. Results

3.1. Concentration-time profiles after IC and IVT injections

The concentration–time profiles after IC (30 nmol) and IVT (150

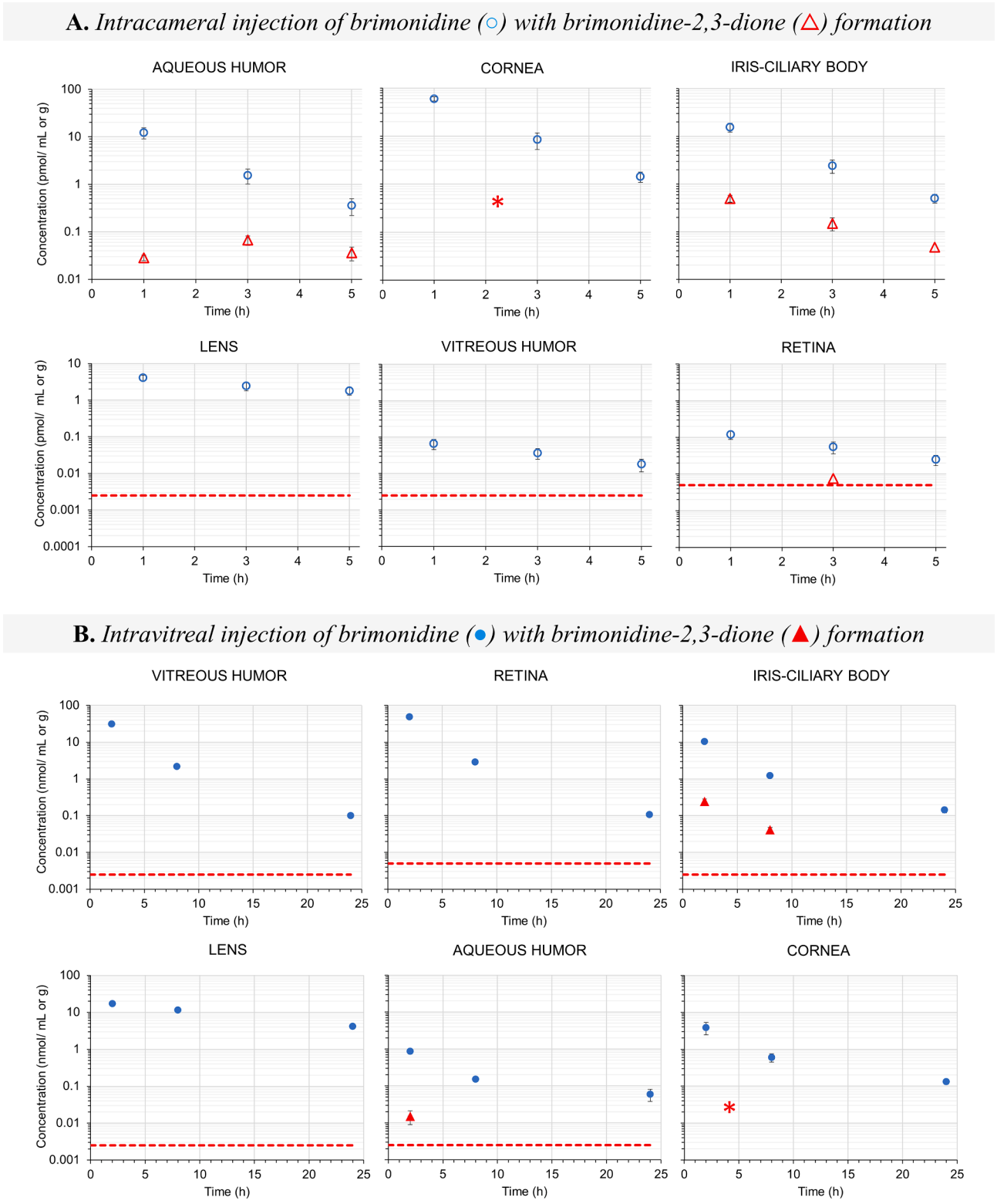

Fig. 3. Concentration-time profile of brimonidine (circle) and brimonidine-2,3-dione (triangle) (mean concentration ± standard error of the mean) after IC (30 nmol, A) and IVT (150 nmol, B) injections of brimonidine tartrate, red dashed lines correspond to LLOQ of the metabolite. The asterisk (*) indicates that the metabolite could not be measured in the cornea due to problems in metabolite extraction from this tissue.

nmol) injections of each parent drug and the ones corresponding to its metabolites are presented in Figs. 2–5. The concentration profiles of cefuroxime axetil are dose-normalized (Fig. 4) to the aforementioned doses for comparative purposes. The original concentration profiles are presented in Appendix A Fig. S1.

In Figs. 2–5 and Tables 1 and 2, the order of tissues starts with the injected tissue followed by the tissues that are exposed to the drug after injection. Metabolites were detected for all parent drugs in two or more

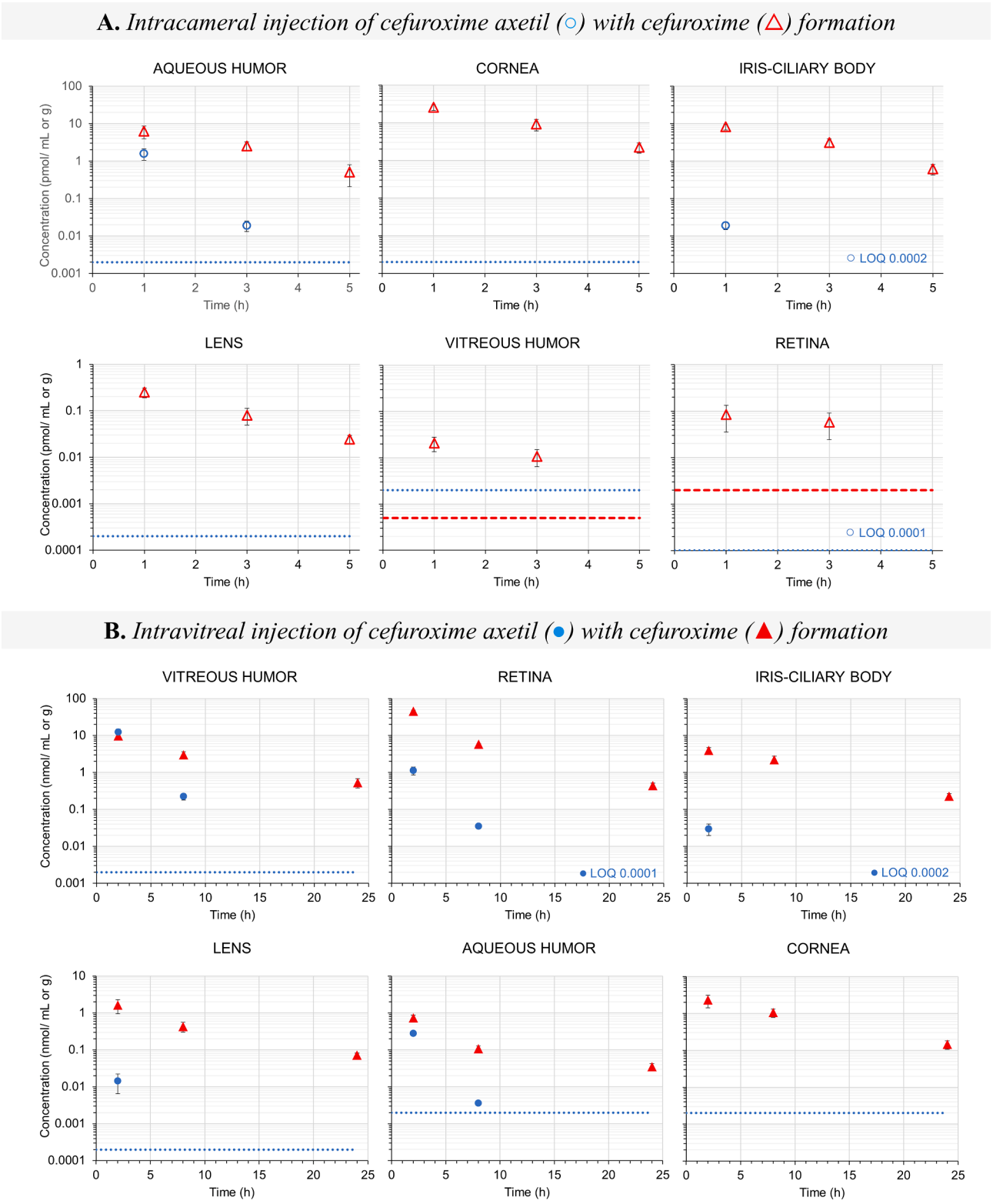

Fig. 4. Concentration-time profile of cefuroxime axetil (circle) and cefuroxime (triangle) (mean concentration ± standard error of the mean) after IC (dose normalized to 30 nmol, A) and IVT (dose normalized to 150 nmol, B) injections. The concentrations profiles corresponding to the original administered doses are presented in Fig. S1. Blue dotted and red dashed lines correspond to the LLOQ of the parent drug and metabolite, respectively. The actual LLOQ value is shown when it is below the lowest concentration on the y-axis.

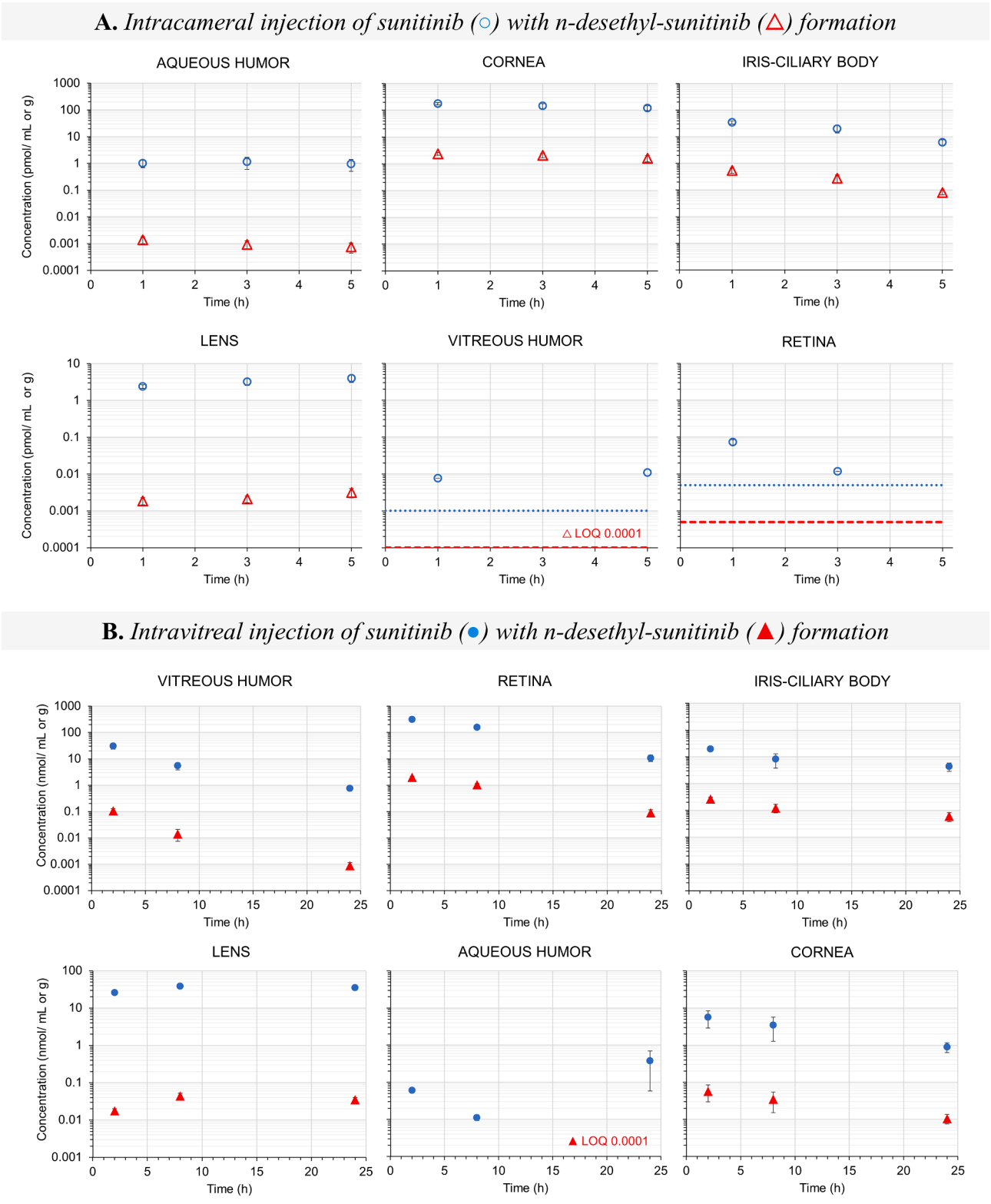

Fig. 5. Concentration-time profile of sunitinib (circle) and N-desethyl-sunitinib (triangle) (mean concentration ± standard error of the mean) after sunitinib malate IC (30 nmol, A) and IVT (150 nmol, B) injections. Blue dotted and red dashed lines correspond to the LLOQ of the parent drug and metabolite, respectively. The actual LLOQ value is shown when it is below the lowest concentration on the y-axis.

Table 1
The $AUC_{0\text{-tlast}}$, $AUC_{t1\text{-tlast}}$, and elimination $t_{1/2}$ parameters of parent drug and metabolites after IC injection (30 nmol into AH) from NCA analysis. AH: aqueous humor; ICB: iris-ciliary body and VH: vitreous humor.

Intracameral injection												
	Acetaminophen						**Acetaminophen sulfate**					
	AH	CORNEA	ICB	LENS	VH	RETINA	AH	CORNEA	ICB	LENS	VH	RETINA
$t_{1/2}$ (min)	44	45	46	*NR*	112	*NR*	*NR*	*NR*	78	*NR*	*NR*	205
$AUC_{0\text{-tlast}}$ (min·nmol/mL)	3205	3418	1243	706	24.7	26.5	31.7	295	66.9	3.48	0.30	1.22
$AUC_{t1\text{-tlast}}$ (min·nmol/mL)	1059	2295	840	594	20.2	21.9	26.9	249	51.1	3.06	0.27	1.10
	Brimonidine						**Brimonidine-2,3-dione**					
	AH	CORNEA	ICB	LENS	VH	RETINA	AH	CORNEA	ICB	LENS	VH	RETINA
$t_{1/2}$ (min)	47	45	49	*NR*	*NR*	107	*NR*		71			
$AUC_{0\text{-tlast}}$ (min·nmol/mL)	2012	5428	1462	758	11.1	18.1	12.5		60.4			
$AUC_{t1\text{-tlast}}$ (min·nmol/mL)	720	3631	995	636	9.15	14.6	11.7		45.5			
	Cefuroxime axetil						**Cefuroxime**					
	AH	CORNEA	ICB	LENS	VH	RETINA	AH	CORNEA	ICB	LENS	VH	RETINA
$t_{1/2}$ (min)	19[a]						66	68	64	71	*NR*	*NR*
$AUC_{0\text{-tlast}}$ (min·nmol/mL)	389[a]						836	3298	1073	31.2	2.45[a]	10.9[a]
$AUC_{t1\text{-tlast}}$ (min·nmol/mL)	14.1[a]						216	842	275	7.89	0.61[a]	2.80[a]
	Sunitinib						**N-desethyl-sunitinib**					
	AH	CORNEA	ICB	LENS	VH	RETINA	AH	CORNEA	ICB	LENS	VH	RETINA
$t_{1/2}$ (min)	2920	453	96				*NR*	*NR*	88			
$AUC_{0\text{-tlast}}$ (min·nmol/mL)	315	40,552	5673	844[b]			0.25	557	83.1	0.61[b]		
$AUC_{t1\text{-tlast}}$ (min·nmol/mL)	255	35,280	4630	772[b]			0.22	486	66.8	0.55[b]		

NR: not reported because the terminal phase of the concentration–time profiles was shorter than two half-lives.
[a] Concentration profile till 180 min (Fig. 4A).
[b] Ascending concentration profile (Fig. 5A).

Table 2
The $AUC_{0\text{-tlast}}$, $AUC_{t1\text{-tlast}}$, and elimination $t_{1/2}$ parameters of parent drug and metabolites after IVT administration (150 nmol into VH) from NCA analysis. VH: vitreous humor, ICB: iris-ciliary body, and AH: aqueous humor.

Intravitreal injection												
	Acetaminophen						**Acetaminophensulfate**					
	VH	RETINA	ICB	LENS	AH	CORNEA	VH	RETINA	ICB	LENS	AH	CORNEA
$t_{1/2}$ (h)	2.97	3.38	4.77	*NR*	6.75	6.51	4.61	4.49	5.70	*NR*	*NR*	6.56
$AUC_{0\text{-tlast}}$ (h·nmol/mL)	170	72.2	42.0	119	6.78	16.9	0.90	2.14	0.85	0.92	0.17	0.81
$AUC_{t1\text{-tlast}}$ (h·nmol/mL)	68.3	49	30.5	107	5.36	13.3	0.9	1.65	0.71	0.87	0.16	0.76
	Brimonidine						**Brimonidine-2,3-dione**					
	VH	RETINA	ICB	LENS	AH	CORNEA	VH	RETINA	ICB	LENS	AH	CORNEA
$t_{1/2}$ (h)	3.60	3.39	5.12	*NR*	*NR*	7.37			2.33[a]			
$AUC_{0\text{-tlast}}$ (h·nmol/mL)	177	160.0	44.1	218	4.89	19.3			0.94[a]			
$AUC_{t1\text{-tlast}}$ (h·nmol/mL)	76.3	111	33.7	201	4.02	15.4			0.69[a]			
	Cefuroxime axetil						**Cefuroxime**					
	VH	RETINA	ICB	LENS	AH	CORNEA	VH	RETINA	ICB	LENS	AH	CORNEA
$t_{1/2}$ (h)	1.02[a]	1.15[a]			0.95[a]		6.40	4.29	4.86	6.24	*NR*	5.57
$AUC_{0\text{-tlast}}$ (h·nmol/mL)	70.5[a]	2.90[a]			0.67[a]		67.4	195	36.2	10.26	3.74	19.05
$AUC_{t1\text{-tlast}}$ (h·nmol/mL)	5.96[a]	0.60[a]			0.13[a]		19.2	49.9	10.75	2.88	1.00	5.59
	Sunitinib						**N-desethyl-sunitinib**					
	VH	RETINA	ICB	LENS	AH	CORNEA	VH	RETINA	ICB	LENS	AH	CORNEA
$t_{1/2}$ (h)	5.64	4.15	*NR*	*NR*	*NR*	–	3.99	4.51	*NR*	*NR*		*NR*
$AUC_{0\text{-tlast}}$ (h·nmol/mL)	210	2546	197	805	3.35[b]	62.7	0.46	17.1	2.82	0.84		0.65
$AUC_{t1\text{-tlast}}$ (h·nmol/mL)	465	2233	178	779	3.29[b]	57.1	0.35	15.1	2.55	0.82		0.59

NR, not reported because the terminal phase of the concentration–time profiles was shorter than two half-lives.
[a] Concentration profile till 8 h (Fig. 3B and Fig. 4B).
[b] Ascending concentration profile (Fig. 5B).

Table 3
NCA primary pharmacokinetic parameters of the parent compounds after IC and IVT injections.

	Acetaminophen	Brimonidine	Cefuroxime axetil	Sunitinib
	IC injection			
V_{ic} (µL)	528	911	*NR* [a]	*NR* [b]
CL_{ic} (µL/min)	9.28	14.7	*NR* [a]	*NR* [b]
	IVT injection			
V_{ivt} (mL)	2.11	2.29	*NR* [a]	3.73
CL_{ivt} (mL/h)	0.881	0.843	*NR* [a]	0.693

[a] NR, not reported because they were based on only two concentration–time points.
[b] NR, not reported because of a concentration-profile shorter than one half-life.

tissues. Nevertheless, the metabolite concentrations were low, except for cefuroxime axetil prodrug that was almost completely converted to cefuroxime during the time scale of the study (Fig. 4). Only low levels of cefuroxime axetil were detected at the earliest time points (Fig. 4).

3.2. Pharmacokinetic parameters after IC and IVT injections

The primary pharmacokinetic parameters of the parent drugs acetaminophen, brimonidine, and sunitinib and the prodrug cefuroxime axetil after IC and IVT administrations are presented in Table 3. The parameters are based on the parent drug concentrations in the aqueous humor (IC injection) and vitreous (IVT injection). Only V_{ic} and CL_{ic} could be estimated for acetaminophen and brimonidine (Table 3), while V_{ivt} and CL_{ivt} could be estimated for the previous compounds and sunitinib (Table 3).

The secondary pharmacokinetic parameters, AUC, and elimination half-lives are reported in Tables 1 and 2. Many $AUC_{0-\infty}$ values were not reliable because the terminal phase of the concentration–time profiles was shorter than two half-lives and therefore this parameter was not reported for any of the compounds. In general, the AUC values were larger for the parent drug compared to the metabolite after IC (Table 1) and IVT (Table 2) administrations. However, this was not the case for cefuroxime axetil, due to its rapid conversion into cefuroxime. Only the cefuroxime $t_{1/2}$ and AUC could be reported for most of the tissues after IC injection (Table 1) and IVT injection (Table 2) but not for cefuroxime axetil.

The ratios between the $AUC_{0\text{-tlast}}$ of the metabolite and the parent drug in the ocular tissues are presented in Fig. 6, except for cefuroxime axetil. The AUC ratios are very low for the SULT, AOX, and CYP3A substrates (less than 0.09) reflecting a low level of drug metabolism, while cefuroxime axetil was converted to cefuroxime at a high extent, suggesting high esterase activity in the ocular tissues. The $AUC_{0\text{-tlast}}$ for cefuroxime axetil could not be determined in most tissues (Fig. 7,

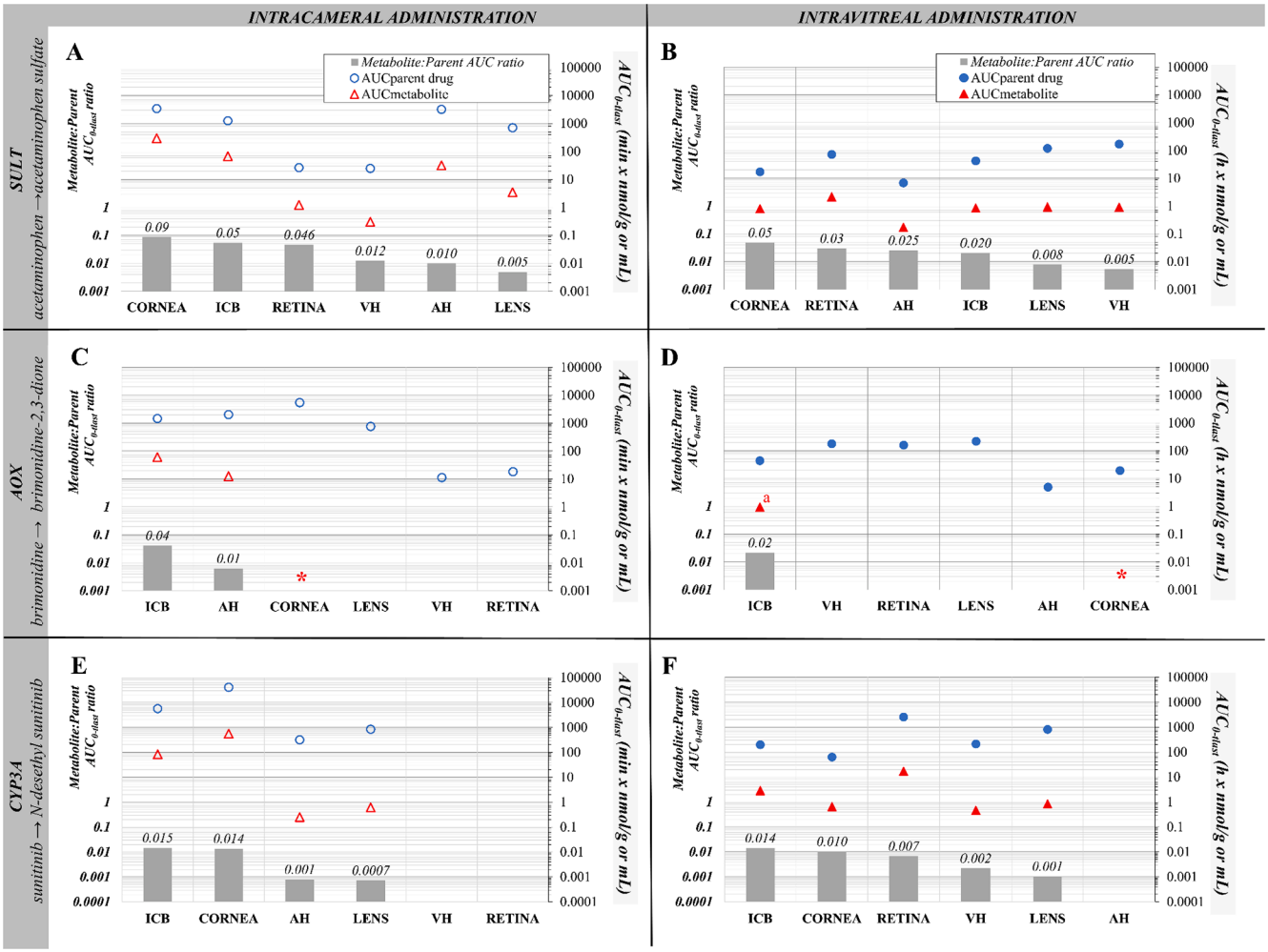

Fig. 6. The AUC $_{0\text{-tlast}}$ of the parent drug and the corresponding metabolite and the metabolite/parent drug ratio of AUC $_{0\text{-tlast}}$ in descending order, after IC (dose 30 nmol) and IVT (dose 150 nmol) administrations. In CD plots, the asterisks* indicate that the metabolite could not be measured in the cornea due to problems in metabolite extraction in this tissue, and "a" informs that AUC $_{0\text{-tlast}}$ is based on the two-initial concentration–time points (see Fig. 3). AH: aqueous humor; ICB: iris-ciliary body and VH: vitreous humor.

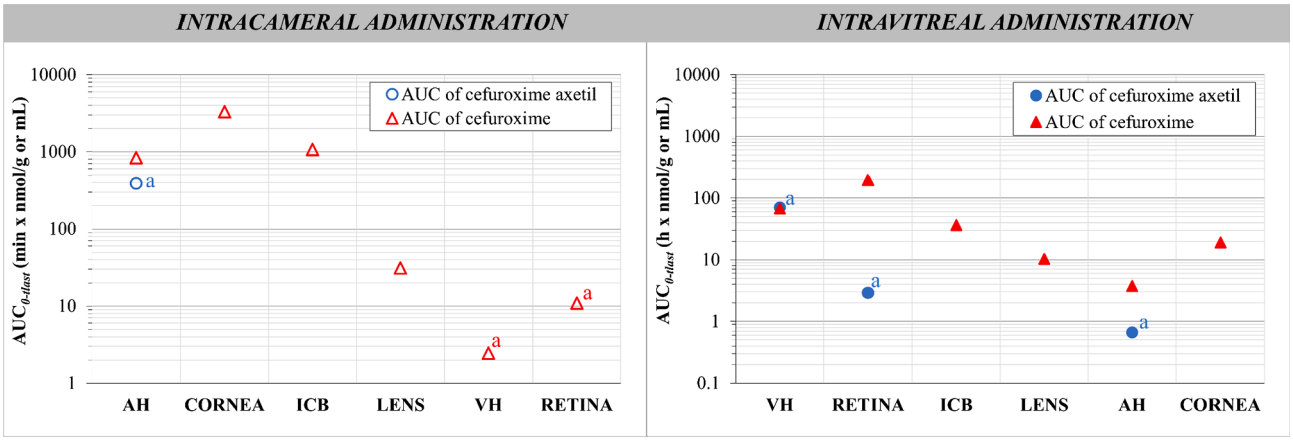

Fig. 7. The $AUC_{0\text{-}tlast}$ of the cefuroxime axetil (circles) and cefuroxime (triangles) after IC injection (dose normalized to 30 nmol) and after IVT injection (dose normalized to 150 nmol) in the six tissues following the anatomical order of the drug disposition. "a": $AUC_{0\text{-}tlast}$ estimated based on the two-initial concentration–time points of the compound (see Fig. 4). AH: aqueous humor; ICB: iris-ciliary body and VH: vitreous humor.

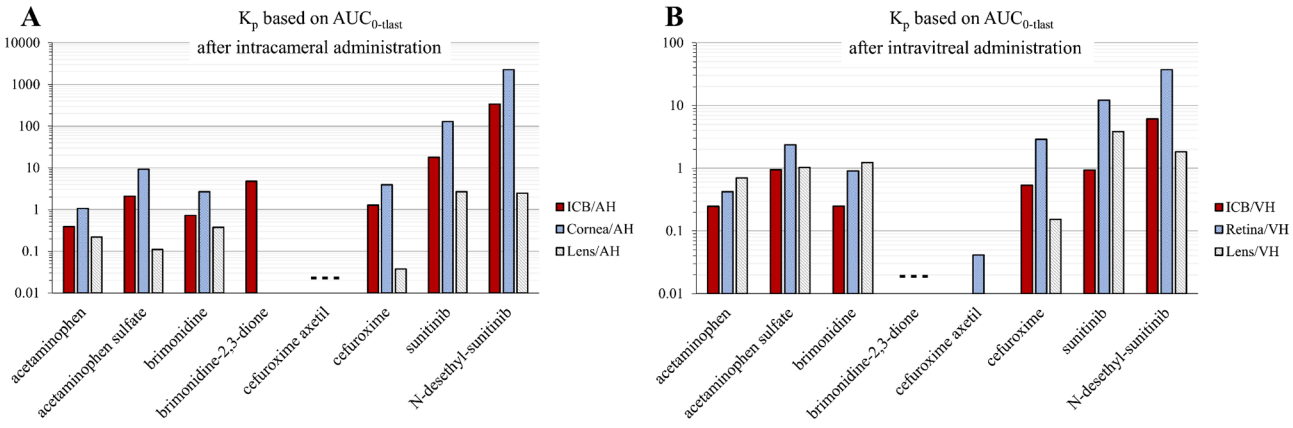

Fig. 8. The K_p values of the eight compounds after IC (**A**) and IVT (**B**) administrations, the dashed line indicates that the compound was not detected in the injected ocular humor. AH: aqueous humor; ICB: iris-ciliary body and VH: vitreous humor.

Tables 1 and 2), because cefuroxime axetil was totally converted to cefuroxime by the end of the *in vivo* study.

The K_p (equation (1)) of the eight compounds between the injected tissues (aqueous humor, vitreous) and their surrounding tissues are presented in Fig. 8 and Table S5. The K_p values after IC injections range from 0.04 (Lens:AH K_p of cefuroxime) to 2249 (Cornea:AH K_p of N-desethyl-sunitinib), while the range for IVT injection was narrower from 0.04 (Retina:VH K_p of cefuroxime axetil) to 37 (Retina:VH K_p of N-desethyl-sunitinib). The compound partitioning after IC injection into the cornea (Fig. 8A, blue bars) is obvious for both drug and metabolite. In the case of IVT injection, partitioning into retina dominates (Fig. 8B, blue bars), though in some cases lens partitioning (Fig. 8B, white bars) was also important.

4. Discussion

In the present study, a cocktail administration was used to deliver four drugs (acetaminophen, brimonidine tartrate, cefuroxime axetil, sunitinib malate) to investigate ocular pharmacokinetics in rabbits after IC and IVT injections. This is one of the most comprehensive *in vivo* ocular pharmacokinetic studies and includes investigation on drug metabolism in the eye. Here, valuable primary pharmacokinetic parameters for these drugs are published for the first time. The cocktail approach shows the benefit of decreasing interindividual and analytical-related variability, providing comparative pharmacokinetic data among the investigated compounds (Fayyaz et al., 2021, 2020).

The pharmacokinetic data requires careful interpretation since not only the enzymatic activity in the ocular tissues is involved, but also the distribution and clearance of the parent drug and the metabolite. The physicochemical properties such as lipophilicity of the compound play a role (Del Amo et al., 2015; Fayyaz et al., 2020). Because the metabolites are more hydrophilic than the parent drug (Table S1), they are expected to present slower ocular distribution and clearance (Del Amo et al., 2015; Fayyaz et al., 2020). Moreover, the continuous formation of the metabolite from the parent drug may also contribute to its longer tissue half-life as seen for some metabolites (acetaminophen sulfate and brimonidine-2,3-dione). We may assume that the ratio of metabolite/drug exposures (AUC ratios) mostly reflect the enzymatic activity. The back-diffusion of metabolites into the injected compartments is likely from the non-vascularized tissues (cornea, lens), but probably not from the vascularized iris-ciliary body and retina. We discuss the specifics of the generated pharmacokinetic data of each compound hereinafter and compare our findings to the published information on relevant ocular enzymes (Table S6).

4.1. Acetaminophen

The V_{ic} and CL_{ic} values of acetaminophen were in the typical range of intracameral pharmacokinetic parameters (V_{ic} = 687–1421 µL; CL_{ic} = 6.44–32.2 µL/min) (Fayyaz et al., 2020), Acetaminophen has a CL_{ic} of 9.28 µL/min that is higher than aqueous humor outflow (3 µL/min) (Del Amo et al., 2015; Kinsey and Barany, 1949), suggesting moderate

clearance via iris-ciliary body blood flow. However, the CL_{ivt} was at the high end (0.881 ml/h) of IVT clearance values in rabbits (0.031–0.753 ml/h) (Del Amo et al., 2015). The V_{ivt} was similar to the anatomical volume of rabbit vitreous of 1.5 ml (Del Amo et al., 2015; Green et al., 1957).

Overall, SULT-mediated metabolism in the eye was low after IC and IVT injections, suggesting that other elimination mechanisms (crossing blood-ocular barriers, aqueous humor outflow) are more important.

After IC injection, SULT activity (based on the metabolite/drug AUC ratios) seems the highest in the cornea followed by the iris-ciliary body and retina. The acetaminophen partitioning in the cornea (cornea:AH K_p) was > 1 and much higher (>9) for the metabolite probably due to the contribution by the metabolism in this tissue (Fig. 8A). On the other hand, the metabolism in aqueous humor seems to be low (AUC ratio = 0.01), and even this value is probably affected by the back-diffusion of the metabolite from the cornea.

After IVT injection, the SULT activity appears low in the vitreous and higher in the cornea and retina (Fig. 6B). While the lens shows one of the lowest SULT activities, acetaminophen partitioning into this tissue is somewhat larger ($K_p = 0.7$) compared to the retina ($K_p = 0.42$) and iris-ciliary body ($K_p = 0.25$), but unlike in the lens, blood flow eliminates drugs and metabolites from the retina and iris-ciliary body. Low level of SULT activity is also shown in aqueous humor and iris-ciliary body, but the AUC ratio in aqueous humor of 0.025 is partly influenced by metabolite diffusion from the vitreous.

These findings match with the only report on SULT activities in rabbit tissues: the highest ocular activities were found in cornea and iris-ciliary body, followed by retina and choroid while activity was absent in the lens (Watkins et al., 1991). To our knowledge, there are no data available on SULT protein expression in the rabbit eye, but these enzyme activities align well with global human proteomics data. SULT isozymes were detected (but not quantified) in human cornea, aqueous humor, iris-ciliary body, vitreous and retina, but not in the lens (Ahmad et al., 2018). Acetaminophen metabolism also produces glucuronide conjugates. UGT activities towards l-naphthol, morphine, and p-nitrophenol have been detected in the cornea, while negligible activities were found in other eye tissues (Watkins et al., 1991). Glucuronides were not investigated in this study, since the expression of human UGTs in the eye is more limited than that of SULTs (Ahmad et al., 2018).

4.2. Brimonidine tartrate

Brimonidine presented a V_{ic} of 911 μL higher than the anatomical volume of rabbit aqueous humor (~300 μL) (Conrad and Robinson, 1977). Also, CL_{ic} (14.7 μL) was much higher that aqueous humor flow rate (≈ 3 μL/min). This is explained by the lipophilicity of brimonidine and its permeability across the blood-aqueous barrier. Also, clearance of brimonidine from the vitreous was in the high end of reported intravitreal clearance range (Del Amo et al., 2015).

Brimonidine is oxidized by AOX to brimonidine-2,3-dione, but metabolite levels were low compared to the parent drug after both IC and IVT injections. Other metabolites such 2-oxobrimonidine, 3-oxobrimonidine and 2,3-dioxobrimonidine have been also observed in the rabbit conjunctiva, iris-ciliary body and cornea (Acheampong et al., 1995, 2002b) but not in aqueous humor (Acheampong et al., 1995) after topical application. However, in another topical multidose study in pigmented rabbits, the metabolites were detected in aqueous humor (Acheampong et al., 2002b). Whether this arises from metabolite diffusion from cornea after repeated topical installations or from slow metabolism in the aqueous humor is difficult to assess. Here, AOX activity after IC administration was observed in the iris-ciliary body, while negligible AUC ratio (0.01) was found in the aqueous humor. The metabolite partition into the iris-ciliary body was determined (K_p = 4.82) but it was unavailable for cornea since brimonidine-2,3-dione could not be extracted from this tissue. Therefore, we cannot exclude the possibility of metabolic activity in the cornea observed by Acheampong et al. (Acheampong et al., 2002b, 1995). No metabolite was found in aqueous humor after IVT injection which supports the lack of aqueous humor AOX activity. Also, after IVT injection AOX activity was seen in the iris-ciliary body, but not in vitreous, retina or lens. Tissues from bovine and rabbit eyes have shown AOX activity, as measured by reduction of nicotinamide N-oxide, in the decreasing order of iris-ciliary body > retina > choroid > cornea > lens (Shimada et al., 1987), while global human proteomics indicates presence of AOX in human retina (Ahmad et al., 2018).

4.3. Cefuroxime axetil

Due to the rapid overall conversion of cefuroxime axetil to cefuroxime after both intraocular injections, we could not estimate the primary pharmacokinetic parameters of cefuroxime axetil. Vitreal AUC values for cefuroxime and cefuroxime axetil were in the same range after IVT injection, whereas after IC injection, the AUC of cefuroxime exceeded that of cefuroxime axetil by > 2-fold. These results suggest that major part of cefuroxime axetil is eliminated via metabolism instead of other elimination mechanisms, even though the ocular clearance of hydrophilic cefuroxime is probably lower than that of the lipophilic prodrug cefuroxime axetil.

Considering the metabolite levels in the tissues, cornea, iris-ciliary body and aqueous humor had the highest hydrolytic activities, with higher partitioning into cornea (>3) than into iris-ciliary body (>1) of cefuroxime. After IVT injection, the highest partitioning was into the retina (>2.5) along with the highest hydrolytic activity, followed by vitreous and iris-ciliary body. The hydrolytic activity of rabbit ocular tissues using a generic esterase substrate *p*-nitrophenyl acetate (NPA) was presented earlier (Hammid et al., 2021; Heikkinen et al., 2018). In both papers, comparable rates of NPA hydrolysis rates were observed among cornea, iris-ciliary body, aqueous humor and vitreous while retina and lens showed about 2-fold and 10-fold lower specific activities, respectively. The carboxylesterase isozymes CES1 – CES3 have been quantitated in several ocular tissues (Hammid et al., 2021). CES1 content in cornea, aqueous humor, vitreous and retina seems to match the above NPA hydrolysis rates (Hammid et al., 2021; Heikkinen et al., 2018) and the tissues with the highest cefuroxime levels in the present study (Fig. 7). However, we cannot exclude the participation of other non-specific ocular esterases in the formation of cefuroxime, or its diffusion between the tissues. In human tissues, CES1 was detected in human global proteomics in all ocular tissues except the aqueous humor and various arylesterases, cholinesterases and paraoxonases were also detected in most of the human ocular tissues except lens (Ahmad et al., 2018).

4.4. Sunitinib malate

Sunitinib is the most lipophilic drug among the compounds injected, and this is reflected in the peculiar pharmacokinetic profiles and the high Kp values that sunitinib exhibit compared to the other three drugs. After IC injection, sunitinib levels in aqueous humor were very low ~1 pmol/mL at one hour after dosing and remained at the same level even at 5 h. With such a shallow profile, V_{ic} and CL_{ic} could not be reliably calculated, but we can anticipate very high V_{ic} (about 1–2 orders higher than anatomical volume of aqueous humor) due to the high K_p values of sunitinib for cornea (>120) and iris-ciliary body (>10). The metabolite levels and the AUC ratios were more than 10-fold higher in the iris-ciliary body and cornea as compared to aqueous humor and lens. This suggests significant CYP3A activity in these tissues, whereas no metabolite was detectable in the vitreous and retina (Fig. 6E). Diffusion of N-desethyl sunitinib from the cornea into aqueous humor is also likely.

After IVT injection, high tissue partitioning of sunitinib (K_p values of >12 and >3 for retina and lens, respectively, Fig. 8B) resulted in the highest reported V_{ivt} (3.7 ml) for a small-molecule compound (Del Amo et al., 2015). Back-diffusion from the lens into the vitreous and further

into iris-ciliary body can be observed in the terminal phase of the concentration profiles of these tissues. In addition, IVT injected sunitinib also accumulated in the anterior tissues, illustrated for example by the relatively high levels in the cornea. Concentrations in aqueous humor were low but rising at 24 h, probably due to drug diffusion from the cornea. The sunitinib CL_{ivt} (0.693 ml/h) was relatively high (Del Amo et al., 2015) in accordance with its high membrane permeability. The highest metabolism for sunitinib was apparent in iris-ciliary body and cornea, and about 10 times lower in the retina and vitreous. K_p values of N-desethyl sunitinib (>37 in the retina, >6 in the iris-ciliary body, and >1.5 in the lens) were higher than those of the parent drug. These high K_p values of the metabolite reflect high parent drug partitioning to the tissues and metabolic activity in these tissues, in addition to the metabolite partitioning from the vitreous (expected to be low due the hydrophilic nature of the metabolite, Table S1).

Previously, S9 homogenates from rabbit, rat, and human whole eyes showed CYP3A-dependent metabolism of ketoconazole (Cirello et al., 2017), while CYP3A mRNA expression has been detected in rabbit retina and iris-ciliary body (Attar et al., 2005) and the human cornea (Kölln and Reichl, 2012). Human CYP3A4 protein has been detected in the retina but not in aqueous humor, lens, and vitreous (Ahmad et al., 2018). Taken together and barring species differences, our *in vivo* pharmacokinetic findings match these reported expression data well.

4.5. Summary

Overall, the pharmacokinetic data in the present study provide new insights into the distribution and metabolism after intraocular injections. Interestingly, corneal accumulation which is typical for lipophilic drugs after topical and IC administrations seems also relevant for sunitinib and brimonidine after IVT injection. In most cases, drug distribution into the lens was higher after IVT than IC injection even though the initial drug concentrations in the injected tissues (vitreous and aqueous humors respectively) were similar. This is presumably due to the larger posterior surface area of the lens and longer drug exposure time from the vitreal side. Sunitinib and brimonidine showed higher accumulation into the lens than most previously studied drugs (Heikkinen et al., 2020), but the lens distribution was clearly less than the distribution to the cornea and iris-ciliary after IC injections. Interestingly, the distribution of IVT-injected drugs to the iris-ciliary body was lower than after IC injection, presumably due to the different anatomic barriers in the tissue (Del Amo et al., 2015). It is also important to note that blood flow eliminates drugs and metabolites from the vascularized tissues (iris-ciliary body, retina). Elimination from the cornea takes place only by diffusion to the lacrimal fluid and aqueous humor, whereas drug elimination from the lens takes place only by redistribution to the aqueous humor and vitreous.

With the exception of prodrug cefuroxime axetil, the investigated drugs were mostly eliminated by non-metabolic processes, and metabolism played only a minor role in their ocular pharmacokinetics. However, metabolism can be relevant from the ocular toxicity perspective. For example, CYP3A enzymes often form reactive metabolites (Kalgutkar and Dalvie, 2015; Zhou, 2008) and some sulfate conjugates are also toxic (Glatt, 2000). Therefore, local metabolism cannot be neglected in ocular drug discovery and development, especially for long-acting formulations. The cornea and iris-ciliary body appear to be the ocular tissues with the most enzymatic activity, followed by the retina, while the lens and ocular humors seemed to have low activity apart from esterases. In general, metabolite exposure in most tissues was 12–10^3 times smaller than the parent drug exposure.

To our knowledge, no IC or IVT pharmacokinetics studies have been published for any of these parent drugs before. Only IVT pharmacokinetics in monkeys has been published for brimonidine but formulated into a drug delivery system (Tamhane et al., 2021). From the injected solutions herein, the drugs primary pharmacokinetic parameters have been obtained for the first time. These parameters allow pharmacokinetic simulations to guide the design of drug release rates and dosing of new ophthalmic drug delivery systems (Del Amo et al., 2015; del Amo et al., 2017; Subrizi et al., 2019). This may advance the development of new ophthalmic formulations of sunitinib, as an inhibitor of neovascularization in the posterior segment of the eye, and brimonidine, as antiglaucoma or neuroprotective agent, after ocular administrations (IC, IVT, topical or subconjunctival). Currently, some promising intravitreal formulations of these drugs are in phase 2 clinical trials. Moreover, we have shown that the role of ocular metabolism on drug clearance seems to be of low impact except for drugs that are substrates of esterases. The metabolites of all drugs were detected at least in some ocular tissues, and they may have an impact on the toxicity of the compounds in the eye.

CRediT authorship contribution statement

Eva M. del Amo: Formal analysis, Writing – original draft, Writing – review & editing. **Anam Hammid:** Conceptualization, Methodology, Writing – review & editing. **Melanie Tausch:** Methodology, Writing – review & editing. **Elisa Toropainen:** Methodology. **Amir Sadeghi:** Methodology. **Annika Valtari:** Methodology. **Jooseppi Puranen:** Methodology. **Mika Reinisalo:** Methodology. **Marika Ruponen:** Methodology, Writing – review & editing. **Arto Urtti:** Conceptualization, Writing – review & editing. **Achim Sauer:** Conceptualization, Writing – review & editing. **Paavo Honkakoski:** Conceptualization, Writing – review & editing.

Declaration of Competing Interest

The authors declare that they have no known competing financial interests or personal relationships that could have appeared to influence the work reported in this paper.

Acknowledgements

Grant support is provided from the EU-ITN project OCUTHER (H2020- MSCA-ITN-2016, grant number 722717), Doctoral Programme in Drug Research (University of Eastern Finland) and the strategic funding of the University of Eastern Finland.

Appendix A. Supplementary material

Supplementary data to this article can be found online at https://doi.org/10.1016/j.ijpharm.2021.121361.

References

Acheampong, A.A., Shackleton, M., John, B., Burke, J., Wheeler, L., Tang-Liu, D., 2002a. Distribution of brimonidine into anterior and posterior tissues of monkey, rabbit, and rat eyes. Drug Metab. Dispos. 30 (4), 421–429.

Acheampong, A.A., Shackleton, M., Tang-Liu, D.D.S., 1995. Comparative ocular pharmacokinetics of brimonidine after a single dose application to the eyes of albino and pigmented rabbits. Drug Metab. Dispos. 23, 708–712.

Acheampong, A.A., Small, D., Baumgarten, V., Welty, D., Tang-Liu, D., 2002b. Formulation effects on ocular absorption of brimonidine in rabbit eyes. J. Ocul. Pharmacol. Ther. 18 (4), 325–337. https://doi.org/10.1089/10807680260218498.

Ahmad, M.T., Zhang, P., Dufresne, C., Ferrucci, L., Semba, R.D., 2018. The human eye proteome project: updates on an emerging proteome. Proteomics 18 (5-6), 1700394. https://doi.org/10.1002/pmic.201700394.

Argikar, U.A., Dumouchel, J.L., Dunne, C.E., Bushee, A.J., 2017. Ocular non-P450 oxidative, reductive, hydrolytic, and conjugative drug metabolizing enzymes. Drug Metab. Rev. 49 (3), 372–394. https://doi.org/10.1080/03602532.2017.1322609.

Attar, M., Shen, J., Ling, K.-H., Tang-Liu, D., 2005. Ophthalmic drug delivery considerations at the cellular level: drug-metabolising enzymes and transporters. Expert Opin. Drug Deliv. 2 (5), 891–908. https://doi.org/10.1517/17425247.2.5.891.

Cirello, A.L., Dumouchel, J.L., Gunduz, M., Dunne, C.E., Argikar, U.A., 2017. In vitro ocular metabolism and bioactivation of ketoconazole in rat, rabbit and human. Drug Metab. Pharmacokinet. 32, 121–126. https://doi.org/10.1016/j.dmpk.2016.11.001.

Conrad, J.M., Robinson, J.R., 1977. Aqueous chamber drug distribution volume measurement in rabbits. J. Pharm. Sci. 66 (2), 219–224. https://doi.org/10.1002/jps.2600660222.

Dalgaard, L., 2015. Comparison of minipig, dog, monkey and human drug metabolism and disposition. J. Pharmacol. Toxicol. Methods 74, 80–92. https://doi.org/10.1016/j.vascn.2014.12.005.

del Amo, E.M., Rimpelä, A.-K.-K., Heikkinen, E., Kari, O.K., Ramsay, E., Lajunen, T., Schmitt, M., Pelkonen, L., Bhattacharya, M., Richardson, D., Subrizi, A., Turunen, T., Reinisalo, M., Itkonen, J., Toropainen, E., Casteleijn, M., Kidron, H., Antopolsky, M., Vellonen, K.S., Ruponen, M., Urtti, A., 2017. Pharmacokinetic aspects of retinal drug delivery. Prog. Retin. Eye Res. 57, 134–185. https://doi.org/10.1016/j.preteyeres.2016.12.001.

Del Amo, EM, Urtti, A, 2015. Rabbit as an animal model for intravitreal pharmacokinetics: Clinical predictability and quality of the published data. Exp Eye Res 137, 111–124. https://doi.org/10.1016/j.exer.2015.05.003.

Del Amo, E.M., Vellonen, K.S., Kidron, H., Urtti, A., Eva, M., Vellonen, K.S., Kidron, H., Urtti, A., 2015. Intravitreal clearance and volume of distribution of compounds in rabbits: in silico prediction and pharmacokinetic simulations for drug development. Eur. J. Pharm. Biopharm. 95, 215–226. https://doi.org/10.1016/j.ejpb.2015.01.003.

Druzgala, P., Wu, W.-M., Bodor, N., 1991. Ocular absorption and distribution of loteprednol etabonate, a soft steroid, in rabbit eyes. Curr. Eye Res. 10 (10), 933–937. https://doi.org/10.3109/02713689109020329.

Dumouchel, J.L., Chemuturi, N., Milton, M.N., Camenisch, G., Chastain, J., Walles, M., Sasseville, V., Gunduz, M., Iyer, G.R., Argikar, U.A., 2018. Models and approaches describing the metabolism, transport, and toxicity of drugs administered by the ocular route. Drug Metab. Dispos. 46 (11), 1670–1683. https://doi.org/10.1124/dmd.118.082974.

Duvvuri, S., Majumdar, S., Mitra, A.K., 2004. Role of metabolism in ocular drug delivery. Curr. Drug Metab. 5, 507–515. https://doi.org/10.2174/1389200043335342.

Fayyaz, A., Ranta, V.P., Toropainen, E., Vellonen, K.S., Ricci, G.D.A., Reinisalo, M., Heikkinen, E.M., Gardner, I., Urtti, A., Jamei, M., Del Amo, E.M., 2020. Ocular intracameral pharmacokinetics for a cocktail of timolol, betaxolol, and atenolol in rabbits. Mol. Pharm. 17, 588–594. https://doi.org/10.1021/acs.molpharmaceut.9b01024.

Fayyaz, A., Vellonen, K.S., Ranta, V.P., Toropainen, E., Reinisalo, M., Valtari, A., Puranen, J., Ricci, G.D.A., Heikkinen, E.M., Gardner, I., Ruponen, M., Urtti, A., Jamei, M., del Amo, E.M., 2021. Ocular pharmacokinetics of atenolol, timolol and betaxolol cocktail: tissue exposures in the rabbit eye. Eur. J. Pharm. Biopharm. 166, 155–162. https://doi.org/10.1016/j.ejpb.2021.06.003.

Glatt, H., 2000. Sulfotransferases in the bioactivation of xenobiotics. Chem. Biol. Interact. 129 (1-2), 141–170. https://doi.org/10.1016/S0009-2797(00)00202-7.

Green, H., Sawyer, J.L., Leopold, I.H., 1957. Elaboration of bicarbonate ion in intraocular fluids: II. Vitreous humor, normal values. AMA. Arch. Ophthalmol. 57, 85–89. https://doi.org/10.1001/archopht.1957.00930050093017.

Hammid, A., Fallon, J.K., Lassila, T., Salluce, G., Smith, P.C., Tolonen, A., Sauer, A., Urtti, A., Honkakoski, P., 2021. Carboxylesterase activities and protein expression in rabbit and pig ocular tissues. Mol. Pharm. 18 (3), 1305–1316. https://doi.org/10.1021/acs.molpharmaceut.0c0115410.1021/acs.molpharmaceut.0c01154.s001.

Harding, S.M., Williams, P.E., Ayrton, J., 1984. Pharmacology of cefuroxime as the 1-acetoxyethyl ester in volunteers. Antimicrob. Agents Chemother. 25 (1), 78–82. https://doi.org/10.1128/AAC.25.1.78.

Heikkinen, E.M., del Amo, E.M., Ranta, V.P., Urtti, A., Vellonen, K.S., Ruponen, M., 2018. Esterase activity in porcine and albino rabbit ocular tissues. Eur. J. Pharm. Sci. 123, 106–110. https://doi.org/10.1016/j.ejps.2018.07.034.

Heikkinen, E.M., Ruponen, M., Jasper, L., Leppänen, J., Hellinen, L., Urtti, A., Auriola, S., Rautio, J., Vellonen, K.-S., Leppänen, J., Hellinen, L., Urtti, A., Auriola, S., Rautio, J., Vellonen, K.-S., 2020. Prodrug approach for posterior eye drug delivery: synthesis of novel ganciclovir prodrugs and in vitro screening with cassette dosing. Mol. Pharm. 17, 1945–1953. https://doi.org/10.1021/acs.molpharmaceut.0c00037.

Jhajra, S., Ramesh Varkhede, N., Suresh Ahire, D., Vidyasagar Naik, B., Prasad, B., Paliwal, J., Singh, S., 2012. Extrahepatic Drug-Metabolizing Enzymes and Their Significance, in: Encyclopedia of Drug Metabolism and Interactions. Wiley Online Library, pp. 1–99. https://doi.org/10.1002/9780470921920.edm028.

Joussen, A.M., Kruse, F.E., Völcker, H.-E., Kirchhof, B., 1999. Topical application of methotrexate for inhibition of corneal angiogenesis. Graefe's Arch. Clin. Exp. Ophthalmol. 237 (11), 920–927. https://doi.org/10.1007/s004170050387.

Kalgutkar, A.S., Dalvie, D., 2015. Predicting toxicities of reactive metabolite-positive drug candidates. Annu. Rev. Pharmacol. Toxicol. 55 (1), 35–54. https://doi.org/10.1146/annurev-pharmtox-010814-124720.

Kinsey, V.E., Bárány, E., 1949. The rate of flow of aqueous humor; derivation of rate of flow and its physiologic significance. Am. J. Ophthalmol. 32 (6), 189–202. https://doi.org/10.1016/s0002-9394(14)78372-2.

Kölln, C., Reichl, S., 2012. mRNA expression of metabolic enzymes in human cornea, corneal cell lines, and hemicornea constructs. J. Ocul. Pharmacol. Ther. 28 (3), 271–277. https://doi.org/10.1089/jop.2011.0124.

Martignoni, M., Groothuis, G.M.M., de Kanter, R., 2006. Species differences between mouse, rat, dog, monkey and human CYP-mediated drug metabolism, inhibition and induction. Expert Opin. Drug Metab. Toxicol. 2 (6), 875–894. https://doi.org/10.1517/17425255.2.6.875.

Muijsers, R.B.R., Jarvis, B., 2002. Moxifloxacin: In uncomplicated skin and skin structure infections. Drugs 62 (6), 967–973. https://doi.org/10.2165/00003495-200262060-00008.

Nakano, M., Lockhart, C.M., Kelly, E.J., Rettie, A.E., 2014. Ocular cytochrome P450s and transporters: roles in disease and endobiotic and xenobiotic disposition. Drug Metab. Rev. 46 (3), 247–260. https://doi.org/10.3109/03602532.2014.921190.

Redell, M.A., Yang, D.C., Lee, V.H.L., 1983. The role of esterase activity in the ocular disposition of dipivalyl epinephrine in rabbits. Int. J. Pharm. 17 (2-3), 299–312. https://doi.org/10.1016/0378-5173(83)90041-8.

Romanelli, L., Valeri, P., Morrone, L.A., Pimpinella, G., 1991. Ocular disposition of acetaminophen and its metabolites following intravenous administration in rabbits. J. Ocul. Pharmacol. 7 (4), 339–350. https://doi.org/10.1089/jop.1991.7.339.

Shimada, S., Mishima, H., Kitamura, S., Tatsumi, K., 1987. Nicotinamide N-oxide reductase activity in bovine and rabbit eyes. Investig. Ophthalmol. Vis. Sci. 28, 1204–1206.

Sjöquist, B., Basu, S., Byding, P., Bergh, K., Stjernschantz, J., 1998. The pharmacokinetics of a new antiglaucoma drug, latanoprost, in the rabbit. Drug Metab. Dispos. 26, 745–754.

Speed, B., Bu, H.-Z., Pool, W.F., Peng, G.W., Wu, E.Y., Patyna, S., Bello, C., Kang, P., 2012. Pharmacokinetics, distribution, and metabolism of [14C]sunitinib in rats, monkeys, and humans. Drug Metab. Dispos. 40 (3), 539–555. https://doi.org/10.1124/dmd.111.042853.

Subrizi, A., del Amo, E.M., Korzhikov-Vlakh, V., Tennikova, T., Ruponen, M., Urtti, A., 2019. Design principles of ocular drug delivery systems: importance of drug payload, release rate, and material properties. Drug Discov. Today. 24 (8), 1446–1457. https://doi.org/10.1016/j.drudis.2019.02.001.

Tamhane, M., Luu, K.T., Attar, M., 2021. Ocular pharmacokinetics of brimonidine drug delivery system in monkeys and translational modeling for selection of dose and frequency in clinical trials. J. Pharmacol. Exp. Ther. 378 (3), 207–214. https://doi.org/10.1124/jpet.120.000483.

Testa, V., Ferro Desideri, L., Della Giustina, P., Traverso, C.E., Iester, M., 2020. An update on ripasudil for the treatment of glaucoma and ocular hypertension. Drugs Today 56 (9), 599. https://doi.org/10.1358/dot.2020.56.9.3178110.

Vadivelu, N., Gowda, A.M., Urman, R.D., Jolly, S., Kodumudi, V., Maria, M., Taylor, R., Pergolizzi, J.V., 2015. Ketorolac tromethamine - Routes and clinical implications. Pain Pract. 15 (2), 175–193. https://doi.org/10.1111/papr.12198.

van Herwaarden, A.E., Smit, J.W., Sparidans, R.W., Wagenaar, E., van der Kruijssen, C. M.M., Schellens, J.H.M., Beijnen, J.H., Schinkel, A.H., 2005. Midazolam and cyclosporin a metabolism in transgenic mice with liver-specific expression of human CYP3A4. Drug Metab. Dispos. 33 (7), 892–895. https://doi.org/10.1124/dmd.105.004721.

Watkins, J.B., Wirthwein, D.P., Sanders, R.A., 1991. Comparative study of phase II biotransformation in rabbit ocular tissues. Drug Metab. Dispos. 19, 708–713.

Zhang, E.Y., Gale, D., Wu, E.Y., Xiang, C.D., Zhang, T., Carreiro, S., Xiang, C.D., Gale, D., Carreiro, S., Wu, E.Y., Zhang, E.Y., 2008. Drug transporter and cytochrome P450 mRNA expression in human ocular barriers: implications for ocular drug disposition. Drug Metab. Dispos. 36, 1300–1307. https://doi.org/10.1124/dmd.108.021121.

Zhou, S.-F., 2008. Drugs behave as substrates, inhibitors and inducers of human cytochrome P450 3A4. Curr. Drug Metab. 9, 310–322. https://doi.org/10.2174/138920008784220664.